Ray-based seismic modeling of geologic models: Understanding and analyzing seismic images efficiently

Article *in* Interpretation · November 2015

DOI: 10.1190/INT-2015-0061.1

CITATIONS
26

READS
1,198

6 authors, including:

Isabelle Lecomte
University of Bergen
130 PUBLICATIONS **1,825** CITATIONS
SEE PROFILE

Paul Lubrano-Lavadera
SWECO
10 PUBLICATIONS **51** CITATIONS
SEE PROFILE

Ingrid Anell
University of Oslo
26 PUBLICATIONS **397** CITATIONS
SEE PROFILE

Simon John Buckley
Norce Research
98 PUBLICATIONS **1,786** CITATIONS
SEE PROFILE

Ray-based seismic modeling of geologic models: Understanding and analyzing seismic images efficiently

Isabelle Lecomte[1], Paul Lubrano Lavadera[2], Ingrid Anell[3], Simon J. Buckley[4], Daniel W. Schmid[3], and Michael Heeremans[3]

Abstract

Often, interpreters only have access to seismic sections and, at times, well data, when making an interpretation of structures and depositional features in the subsurface. The validity of the final interpretation is based on how well the seismic data are able to reproduce the actual geology, and seismic modeling can help constrain that. Ideally, modeling should create complete seismograms, which is often best achieved by finite-difference modeling with postprocessing to produce synthetic seismic sections for comparison purposes. Such extensive modeling is, however, not routinely affordable. A far more efficient option, using the simpler 1D convolution model with reflectivity logs extracted along verticals in velocity models, generates poor modeling results when lateral velocity variations are expected. A third and intermediate option is to use the various ray-based approaches available, which are efficient and flexible. However, standard ray methods, such as the normal-incidence point for unmigrated poststack sections or image rays for simulating time-migrated poststack results, cannot deal with complex and detailed targets, and will not reproduce the realistic (3D) resolution effects of seismic imaging. Nevertheless, ray methods can also be used to estimate 3D spatial prestack convolution operators, so-called point-spread functions. These are functions of the survey, velocity model, and wavelet, among others, and therefore they include 3D angle-dependent illumination and resolution effects. Prestack depth migration images are thus rapidly simulated by spatial convolution with detailed 3D reflectivity models, which goes far beyond the limits of 1D convolution modeling. This 3D convolution modeling should allow geologists to better assess their interpretations and draw more definitive conclusions.

Introduction

Seismic data are key to retrieving structural and petrological information about the earth's subsurface within a targeted zone. This is most notably evident in oil and gas exploration, but it is also relevant to CO_2 sequestration, mining, geothermal, and various near-surface applications. Seismic interpreters are geoscientists with various backgrounds and need to be acquainted with geology and geophysics. However, geophysicists involved in seismic imaging (Gray, 2001), in charge of producing the seismic sections interpreters will work with, are seldom in direct touch with the latter. Valuable information about what may lie behind the seismic images is not always provided, and although most interpreters are well aware of seismic imaging principles and potential pitfalls, e.g., illumination and resolution issues, this often stays at the theoretical level. When faced with case-by-case interpretation issues, an interpreter may want to be more confident about geologic models. Seismic modeling is therefore a very useful tool for conceptual testing, as long as an appropriate method is used and all necessary input information is made available.

Ideally, seismic modeling of geologic models should be a prerequisite to validate seismic interpretation, as is the case in any inversion approach in which data are used to infer a model. Such inversions compare the observed data (here the seismic image) and the modeled one. The discrepancy is then estimated and can be used to update the model if the disagreement is too large, further iterating the process until the best possible convergence between observed and modeled data is found. Though (iterative) inversions may be carried out for some stages of the complex seismic processing se-

[1]NORSAR, Kjeller, Norway and University of Oslo, Department of Geosciences, Oslo, Norway. E-mail: isabelle.lecomte@norsar.com; isabelle.lecomte@geo.uio.no.
[2]NORSAR, Kjeller, Norway. E-mail: paul.lubrano@norsar.com.
[3]University of Oslo, Department of Geosciences, Oslo, Norway. E-mail: i.m.anell@geo.uio.no; daniel.schmid@geo.uio.no; michael.heeremans@geo.uio.no.
[4]Uni Research, CIPR, Bergen, Norway. E-mail: simon.buckley@uni.no.

Manuscript received by the Editor 22 March 2015; revised manuscript received 10 July 2015; published online 25 September 2015. This paper appears in *Interpretation*, Vol. 3, No. 4 (November 2015); p. SAC71–SAC89, 20 FIGS., 2 TABLES.
http://dx.doi.org/10.1190/INT-2015-0061.1.

quence, this is seldom performed at the interpretation level. Key issues relate to the appropriate seismic modeling method to use and the cost of modeling, which is a critical resource question during exploration and production.

Among the various existing modeling methods (e.g., Fagin, 1991; Behzad, 2012), we will only refer to two main classes here: the so-called full-wavefield ones, among which finite-difference (FD) modeling is best known and used — thus considered here as the reference for that class — and ray-based (RB) approaches. These two classes cover methods of modeling general 2D and 3D structures as is our interest here. Note that in 1D models, i.e., horizontally stratified structures without lateral velocity variations, so-called reflectivity methods (e.g., Sen, 2014) should be used instead because these methods accurately calculate all wave types with a relatively small computation effort.

Beyond conventional approaches, of interest for interpretation work and which will thus be mentioned, RB modeling is also capable of estimating 3D spatial prestack convolution operators called *point-spread functions* (PSFs; Lecomte and Gelius, 1998; Lecomte, 2008a). PSFs can then be used to rapidly simulate prestack depth migration (PSDM) images, without generating synthetic seismograms and processing them (Lecomte et al., 2003). That specific type of RB modeling is similar in application and efficiency to the well-known 1D convolution modeling method, extensively used in industry. However, such a 3D spatial prestack convolution approach goes beyond the major limits of 1D convolution and provides robust and flexible PSDM modeling, including 3D angle-dependent illumination and resolution effects. The latter are especially important for a better constrained interpretation analysis, as will be illustrated. The FD and RB modeling types are first briefly compared, for the sake of information, before concentrating on the latter type, which is the main focus of the present paper.

Full-wavefield and ray modeling: Both are needed

Full-wavefield methods, such as FD, rely on direct numerical solutions to the wave equation, whereas RB approaches follow ray theory, i.e., high-frequency approximation of this equation. The latter requires new equations to be solved: the eikonal equation for rays and traveltimes and the transport equation for amplitudes along the calculated rays. Both modeling approaches are widely used, with each having inherent advantages and drawbacks. As such, they often complement each other, neither being able to solve all modeling needs alone. A detailed discussion on FD "versus" RB modeling is beyond the scope of this paper, but a few key points should be mentioned.

Table 1 provides a brief comparison of the main features and application domains of FD and RB modeling, intended to show the complementary nature of the methods. FD modeling provides complete seismograms, but with a high associated computing cost and in a "black-box" manner. A velocity model, survey, and wavelet information are input, and all possible waves are then automatically generated, with or without box-boundary contributions (e.g., free-surface effects). Analyzing the propagation may be difficult, even if one can generate animations to visualize the propagation, and only seismograms are produced. RB modeling, in its traditional implementation, rapidly and accurately provides synthetic seismograms for user-selected wave phases (P, S, reflection, transmission, conversion, primaries, multiples, etc.). It may, however, miss several wave types (e.g., headwaves, surface waves, and diffractions), although there are various RB approximations to estimate them too (Gjøystdal et al., 2007). Despite this and in comparison with FD, additional information, such as traveltime, amplitude, polarization, etc., is provided by RB modeling. These propagation parameters are indeed useful beyond seismograms generation, such as for illumina-

Table 1. Comparison between RB and FD modeling.

RB modeling	FD modeling
High-frequency approximation	No high-frequency approximation
Flexible wavefield subselection	Full-wavefield simulations
Missing some wave types, diffraction possible	Contains headwaves, surface waves, diffractions, etc.
Smooth macromodels	Gridded models
Fast and accurate	Time and memory consuming
Target-oriented approach	Whole model (black-box)
Synthetic seismograms for understanding real data	Complete synthetic seismograms for processing tests
Analysis of wavefield parameters	Propagation analyses by movies
Several wavelets	Predefined frequency range
Synthetic seismograms and more	Only synthetic seismograms
Illumination and miscellaneous studies	Benchmark data set
Input parameters for Kirchhoff-based migration methods	Used for full-waveform migration methods

tion studies in survey planning and as input to migration codes (e.g., Laurain et al., 2004; Gjøystdal et al., 2007).

There is no doubt that an ideal modeling approach should consist of generating complete synthetic seismograms, before using them according to the processing sequence of field data. Complete synthetic seismograms in general 2D/3D models are best obtained by FD modeling. FD modeling is thus essential for benchmarking studies (e.g., Arntsen et al., 2007; Johansen et al., 2007) and development of advanced seismic processing techniques. However, FD modeling is a demanding task in terms of time, computer hardware, software, and expertise, and efforts are often joined for 3D as is the case for the SEG Advanced Modeling Corporation (Pangman, 2007). Interpreters and other domain experts who use seismic data will seldom have such possibilities, especially for routine work. We therefore further discuss applications of RB modeling for the specific needs of interpretation, and we include cases that may contribute to improved interpretation skills by applying modeling to diverse geologic models (e.g., outcrop analogs and numerical geologic models).

Ray-based seismic modeling: Beyond seismograms

We intentionally use the term "ray-based" instead of "ray-tracing" modeling to broaden the concept. The term "ray" is used here as a synonym to the underlying high-frequency approximation applied to the wave equation, rather than specifically for the raypath, which is not always calculated in some of the RB methods. This is, for example, the case of the eikonal solvers (e.g., Podvin and Lecomte, 1991), which aim to efficiently and robustly calculate the traveltime of the first arrival for specific applications (refraction seismic, earthquake locations, etc.). Rays are computed only as a by-product if desired. These methods may be indeed sufficient for the convolution approaches we will discuss here. Solving high-frequency approximations of wave equations in classic RB approaches, however, leads to the calculation of other important parameters for each considered wave mode, i.e., not only traveltime but also amplitude, polarization, etc. These parameters are not specifically generated for synthetic seismograms; much can be learned from analyzing them as stand-alone products for a better understanding of wave propagation and waveforms, rays being also a useful visual support of these analyses. Interpreters will benefit from more systematically using RB modeling in its standard forms because such modeling is fast and interactive.

Let us come back to the specific needs of interpreters, which are to obtain rapid modeling results, while still accounting for real (complex) cases with proper propagation and seismic imaging effects. This kind of RB modeling relies on convolution approaches, starting from 1D poststack time cases, and progressing to obtain 3D spatial prestack ones, which allow for a more in-depth understanding of seismic imaging. Some basic elements of seismic modeling by convolution approaches will be briefly reviewed. Because routine seismic processing suppresses multiple arrivals, we limit ourselves to modeling of primary reflections in our examples, though some of the RB methods can deal with multiple reflections in addition. We also use only isotropic cases for the sake of simplicity, although RB modeling handles anisotropy too.

1D time convolution

We need to come back to the basic principles of convolving a 1D function with a wavelet to simulate a seismic trace. This is a correct mathematical principle, widely used in geophysics for decades (Robinson and Treitel, 1978). The method is mathematically simple and thus easily understood and programmed, hence its popularity. The key issues are, however, as follows: (1) how to generate the 1D time function so that it properly represents some recorded/imaged elastic-wave responses, (2) the type of wavelet to use, and (3) the purpose of the generated trace. In standard reflection seismic modeling cases, the 1D time function consists of "spikes" at specific times attached to reflected/diffracted events, their strength being proportional to calculated amplitude values; other propagation effects might be added too, such as attenuation. That 1D time-convolution process is actually fundamental to RB-modeled synthetic seismograms: the calculated traveltimes of the considered waves, in prestack modes (i.e., modeling "raw" recordings), define the spike locations of the time function and other parameters constrain the strength and shape of the signals for each wave. This leads to synthetic data that can be used for processing tests, wave phase identifications, etc. In the following, however, we will first consider the specific case of modeling poststack seismic, which is more suited for interpretation, showing how the convolution principle is often used in that case.

Modeling poststack seismic with 1D time convolution

In many cases, interpreters will work on poststack time-migrated seismic sections. For flat structures, stacked-only sections can be used without any migration, although that is not recommended. Performing a stack means, in any case, generating seismic sections seemingly corresponding to zero-offset acquisition, i.e., with the source and receiver at the same location, though data originally contain nonzero offset information. To simulate such stacked seismic sections, migrated or not, three RB approaches may be used, two explicit (normal-incidence point [NIP] and image ray [IR]) and one implicit, known as standard *1D convolution* or *1D trace modeling*, although the term of *modeling* is not always well defined in that latter case.

Standard 1D trace modeling

For decades, a dominating model has been the horizontally stratified medium with elastic parameters only varying with depth, i.e., a 1D model. It has been used to design seismic acquisition, processing, imaging, and inversion. With such a model, it is relatively simple to obtain traveltimes of zero-offset primary reflections as the sum of two-way vertical times in each layer, thus obtaining analytically the time function needed for the convolution process. Zero-incidence reflection coefficients are also straightforward to calculate and, when combined with the time function, a reflectivity log is formed, ready to convolve with a wavelet. The obtained zero-offset trace is then representative of a recorded seismogram if the actual structure is 1D, and the source and receiver are colocated. It can also be considered as an ideal time-migrated trace (no other amplitude effects than reflection strength), again if the actual structure is 1D. However, even in this case, although the vertical (time) resolution is properly estimated (function of the frequency content of the considered wavelet), no lateral resolution effects are considered, effects which are inherent to the local focusing in seismic imaging. Horizontal resolution effects are thus often ignored, even though they influence amplitudes and structural information, including in relatively flat cases. When the actual structures are not 1D at all, i.e., with lateral velocity variations, the time function has to be adapted accordingly. However, in 1D trace modeling, traveltimes are often systematically extracted along "vertical" lines, in the best case directly from a previously time-migrated section, but often directly from a depth model or a well log. This may be misleading: zero-offset rays are not vertical in non-1D models. Figure 1 illustrates 1D trace modeling in a simple synthetic model in which reflectivity of a selected modeling target is extracted along vertical lines in depth; we will later see the consequences of that. Note first the structural differences between the true depth-version of the target and the simulated "time-migrated" one.

Let us now review the contribution of standard RB methods for a more appropriate modeling of poststack seismic sections. A discussion on adapted models for such modeling will be given in the next section.

Normal-incidence point method for poststack unmigrated sections

The stacking process of reflection seismic intends to simulate zero-offset acquisition from offset data, while also reducing the data quantity and improving signal-to-noise ratio. RB approaches are especially well adapted to visualize "poststack" propagation. This is because in most cases, zero-offset propagation corresponds to the same raypath, "down" and "up." The reflected ray is perpendicular to the reflector (in isotropic cases), according to Snell's law, and the reflection point is called the NIP. Figure 2 uses the model from Figure 1 and shows such NIP rays for overburden and target reflectors. The corresponding traveltimes are represented as spikograms (spike at the arrival time) for a simple visualization of the corresponding time horizons. Amplitudes and other parameters are also available, however, which can be analyzed and/or used to generate complete stacked sections. NIP modeling can also include diffractions generated at intersections of depth horizons and which will appear as hyperbolic-like features on the spikograms. The reflections on NIP sections may look like geologic time horizons, although there are well-known exceptions (e.g., the classic bow-tie example of a syncline; see later). NIP modeling is indeed only meant to be used for simulating poststack unmigrated time sections, as done in Anselmetti et al. (1997).

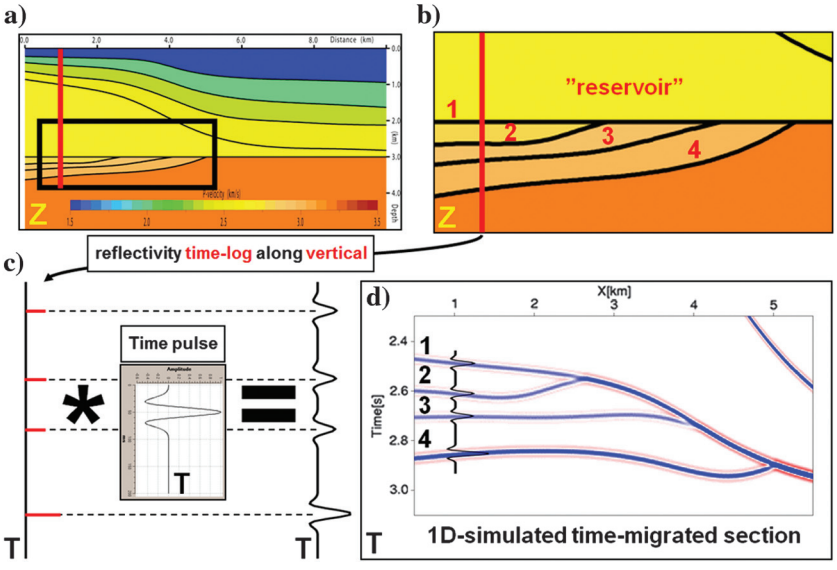

Figure 1. Synthetic model 1, trace modeling from depth model. (a) Overburden with a top water layer and four constant-velocity layers with lateral structural variations; (b) the target has a flat horizontal "erosion" level and three upward-curved horizons truncated at the former, with velocity increasing at each reflector; (c) reflectivity logs in time are extracted along vertical (depth) lines for the target area, converted to time, and convolved with a (time) wavelet; and (d) generating traces in panel (c) for several lateral positions and plotting them side by side gives a time section that is supposed to approximate a poststack time-migrated one.

Image-ray method for poststack time-migrated sections

The IR method is used instead to simulate poststack time-migrated sections, applying a ray concept introduced by Hubral (1977). Although the method re-

lies on approximations, limiting its application to small dips (Black and Brzostowski, 1994), it helps in understanding time-migration effects. The NIP and IR methods are very fast to compute and flexible, and are recommended, especially in 2D, to get a good insight of wave propagation and the possibly complex relationships between time and depth domains, and between unmigrated and migrated time domains. Figure 3 shows the corresponding IR results for the model used in Figures 1 and 2. The rays may look unrealistic, which is a result of them departing perpendicular to the acquisition surface (for explanations, see Hubral, 1977). By collecting two-way traveltimes along these rays at each intersection with a reflector and plotting the latter in spikograms, a simulated poststack time-migrated section is obtained.

Figure 4 shows a comparison of the IR section with that computed from 1D trace modeling (Figure 1). Although the two sections are similar in shape, there are significant misties of the structures, laterally (up to 400 m) and vertically (0.25 s). Although the three diffraction points are at the correct lateral positions in the 1D trace-modeling section, resulting from the reflectivity logs being extracted vertically from the depth model, this is in no way proof of good modeling. Poststack time migration will indeed mislocate these points in a laterally varying velocity model, as properly modeled on the IR section. The only way that 1D trace modeling could reproduce a poststack time-migrated section in non-1D models would be to extract the reflectivity log vertically on the poststack time-migrated section, after interpretation of key horizons in that domain. However, it is far better to use an IR approach instead of 1D trace modeling, at least for target models that are not too detailed or complex. To further illustrate NIP/IR sections, Figure 5 shows another model with the same overburden as in Figures 1–4, but with a deep syncline as the target. The corresponding NIP section shows the well-known bow-tie effect, whereas the IR section shows a closer resemblance to the geologic features. Note, however, how the right side of the syncline, which turns upward in the depth model, appears to be turning downward on the IR section, as may happen with poststack time migration.

3D spatial prestack convolution for prestack depth migration modeling

In complex geologic cases, interpreters should use PSDM sections to avoid significant pitfalls produced by seismic imaging applied in the time domain. This is assuming that the geophysicists are able to define a proper interval-velocity model because PSDM is very sensitive to this input. As we are dealing with modeling,

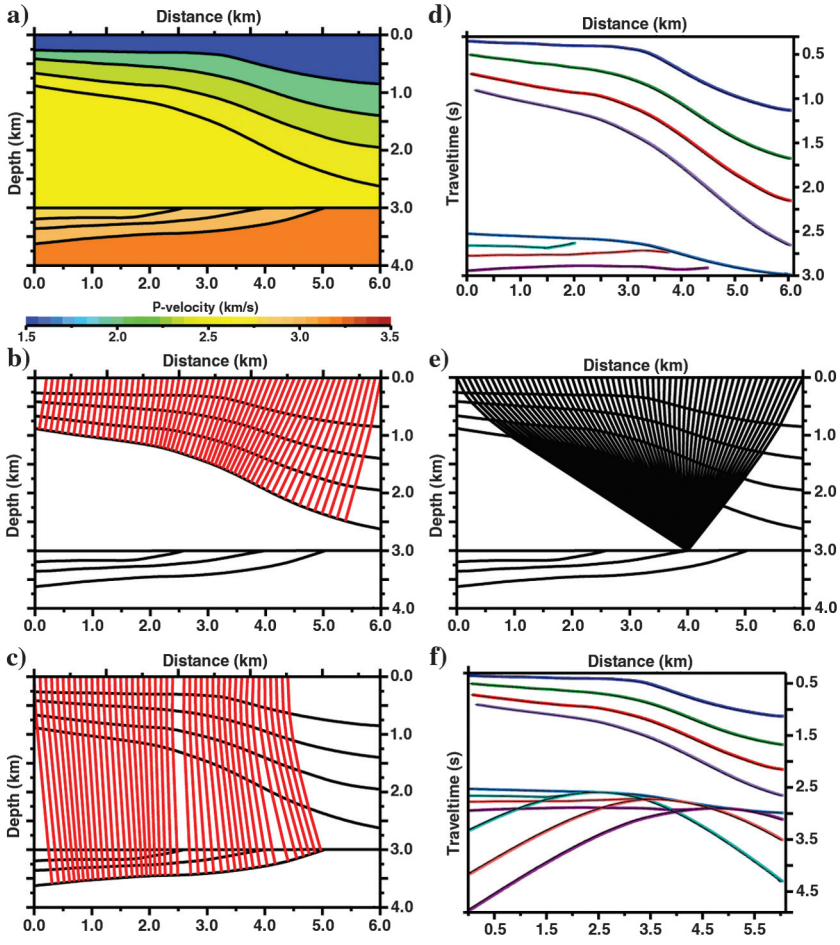

Figure 2. Synthetic model 1, NIP ray tracing: (a) Velocity model, (b) NIP rays for one overburden reflector, (c) NIP rays for one target reflector, (d) traveltimes of all NIP rays (spikograms), (e) diffracted rays from one of the three diffraction points, and (f) spikograms including all diffractions.

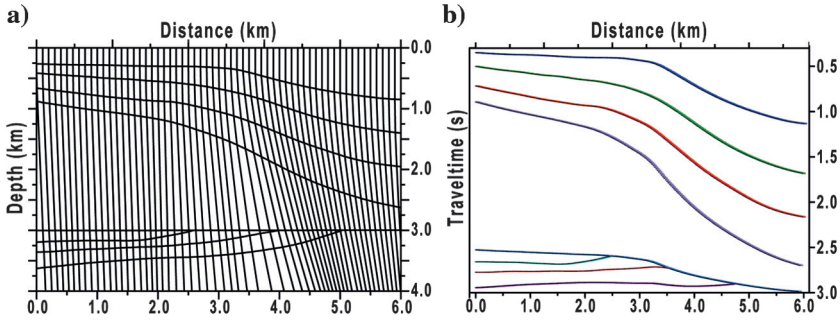

Figure 3. Synthetic model 1, IR tracing. (a) IR rays and (b) corresponding spikograms.

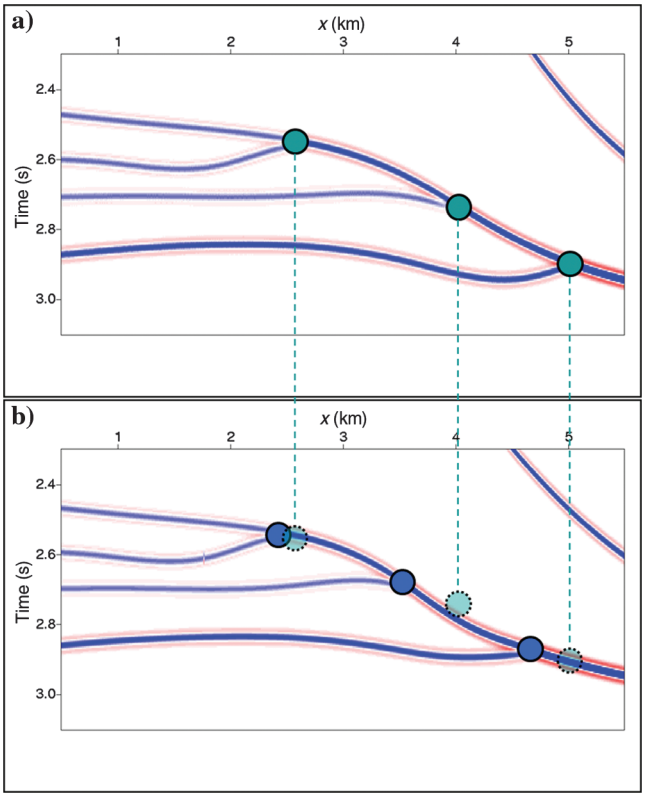

Figure 4. Synthetic model 1, simulation of poststack time-migrated sections. Compare (a) the trace modeling of Figure 1 and (b) the IR section of Figure 3. Compare the positions of the three diffraction points between the two sections.

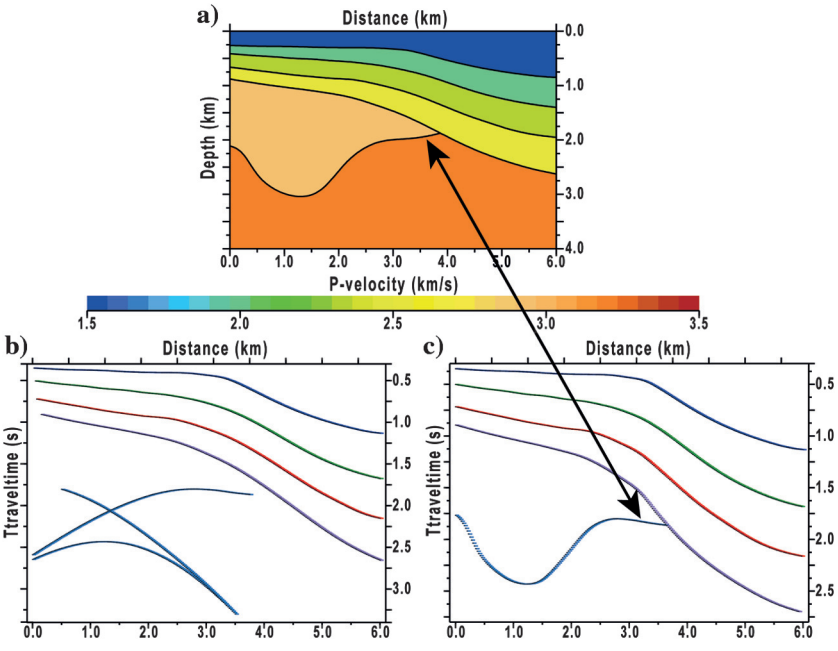

Figure 5. Synthetic model 2. (a) Same overburden as in model 1 (Figures 1–3), but with a syncline as the target; (b) NIP traveltimes with bow-tie effect; and (c) IR traveltimes — compare the syncline shape with panel (a).

we assume in the following that the so-called background velocity model needed for PSDM is provided a priori. We first review key elements of PSDM, before introducing a 3D spatial prestack convolution approach for direct modeling of PSDM sections.

Prestack depth migration: Basic principles

We take a homogeneous isotropic velocity model and consider a point scatterer P (Figure 6). P can also be seen in the following as a reflection point. Because a reflector can be approximated as a set of juxtaposed elementary point scatterers (Huygens' second principle), understanding the images of these is key to understanding seismic reflection images. For a given source/receiver (S-R) pair, the point-scatterer response is recorded at a so-called scattering traveltime T_{S-P-R} corresponding to the sum of the traveltimes from S to P and from P to R; i.e., $T_{S-P-R} = T_{S-P} + T_{P-R}$, whatever paths the waves follow between the points (straight lines in the homogeneous case of Figure 6). Any PSDM method, either RB (Kirchhoff or diffraction-stack type; e.g., Schneider, 1978) or full wavefield, consists of (1) a compensation for the two paths SP and PR (the "backpropagation" part of PSDM), before (2) focusing the recorded seismic energy at each potential scattering point (the "imaging" part of PSDM). Note that for step (1), an accurate velocity model is necessary to perform modeling of the wave propagation between S-P and P-R.

Figure 6a shows first synthetic input data for two simplified acquisition surveys, i.e., common shot and zero offset, to later emphasize survey effects in seismic imaging. Figure 6b shows the spatial loci of points corresponding to constant values of scattering traveltime T_{S-P-R} for a given S-R pair. These curves, called *scattering isochrones*, are ellipses in a homogeneous isotropic model. They are the result of the sum of the circular isochrones (wavefronts) T_{S-P} and T_{P-R} departing from S and R, which are the focal points of these ellipses. When S and R are at the same location (zero offset and poststack equivalent), the ellipses become circles. PSDM projects back the recorded seismic energy along these scattering isochrones, but in a "blind" manner in most methods, especially commercial and industry standard. The energy is spread all along the isochrones because the specific direction the energy is coming from is unknown (Figure 6c). Due to the huge amount of recorded data, one can expect in this summation process a constructive interference at the actual point scatterer P (Figure 6d), and destructive interference elsewhere, although the data quantity in itself is no guarantee of this. The geometric distribution of the S-R pairs,

in combination with the characteristics of wave propagation through the velocity model, as well as the frequency bandwidth of the data, will also influence the quality of the focusing (imaging) process at each considered P, as well as outside the scattering structures. As an example, too coarse S-R sampling will make the scattering isochrones visible on the final seismic image, due to a lack of destructive interference; this is the reason for steep striping noise on many migrated seismic sections, which affects not only image quality, but also the amplitudes of picked reflections.

Figure 6c (left panel) shows the elementary PSDM image for one noncoincident S-R pair, with the ellipse being smeared in a spatially varying pattern as a combination of the wavelet and a pulse-stretching effect. The latter is due to the opening angle between the incoming ray at P and the outgoing one: the larger that angle, the wider the zone around the scattering isochrone is, hence the worse the resolution. An offset-dependent resolution issue will be illustrated later by modeling examples. In the zero-offset case (Figure 6c, right panel), the scattering isochrones remain circular as S and R are coincident. Although the homogeneous point-scatterer model is the same in both cases, the final images are different (Figure 6d). The focusing patterns are not only dissimilar around P, but also away from it, with some large-scale cross patterning due to the lack of destructive interferences of the scattering isochrones attached to the extremities of each survey (limited-aperture effect).

The simple homogeneous example of Figure 6 illustrates several PSDM issues: (1) images depend on survey geometry; (2) resolution varies as a function of offset, as well as a function of opening angle at each image point, and thus varies along the scattering isochrones, even for a constant offset; and (3) limited-aperture effects may spread across a large zone of the image. Therefore, having fast and flexible modeling methods taking into account all these issues, but without performing the expensive "full-wavefield modeling and processing," should help geologists and interpreters to better understand the geology from the seismic images they analyze.

Prestack depth migration modeling by a 3D spatial prestack convolution approach

In an attempt to provide interpreters with a solution to the requirements presented above, RB modeling of PSDM point-scatterer responses have been studied (Lecomte and Gelius, 1998; Lecomte, 2008a). These point-scatterer responses are the PSFs mentioned earlier and are well known in optics, although in seismic imaging, we generally deal with backscattering (two-way energy path) and not direct transmission as in photography or astronomy (the latter case also applies to seismic imaging, i.e., to model tomography responses). Then, having RB-modeled PSFs of PSDM images and recalling Huygens' second principle, which states that reflectors are juxtaposed secondary sources (point scatterers), direct modeling of seismic images is obtained by a 3D spatial prestack convolution between the PSFs and reflectivity models (Lecomte et al., 2003; Lecomte, 2006, 2008b, 2013a, 2013b). Other authors have used full-wavefield modeled PSFs for similar convolution approaches (e.g., Toxopeus et al., 2003). In this work, we compute PSFs from RB algorithms because it allows a faster and more flexible application of the 3D spatial prestack convolution approach.

It is beyond the scope of the present paper to detail the 3D spatial prestack convolution method of choice (we refer to Lecomte, 2008a; Lecomte and Kaschwich, 2008). Figure 7 summarizes the basic elements of such modeling. A given velocity model and a survey are used to generate, via various RB modelings, so-called *illumi-*

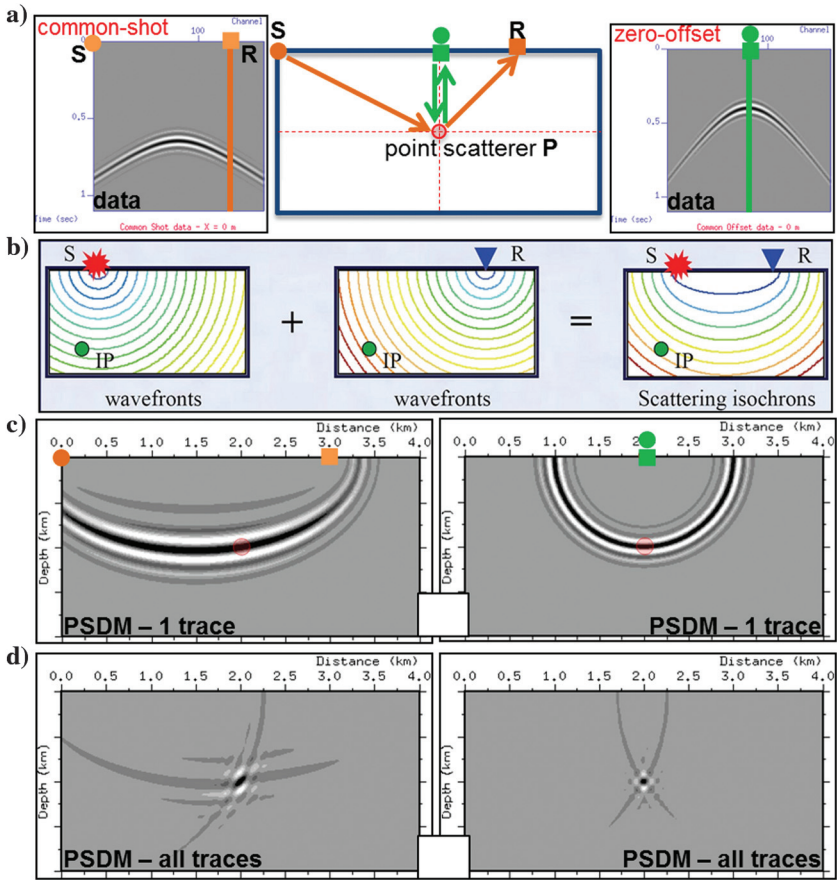

Figure 6. PSDM principles. (a) Point scatterer in homogeneous background velocity with Born-modeled synthetic (left) common-shot and (right) zero-offset gathers; (b) scattering isochrones as sum of wavefronts calculated in background velocity model for a shot (S) and receiver (R) couple, and at all image-point (IP); (c) PSDM response for one trace only and (d) for all traces, for (left) common shot and (right) zero offset.

nation vectors ($\mathbf{I}_{SR}$) at a target point P (Figure 7a), i.e., using a method which can produce the required slowness vectors at that point ($\mathbf{p}_S$ from S to P, and $\mathbf{p}_R$ from P to R); $\mathbf{I}_{SR} = \mathbf{p}_R - \mathbf{p}_S$. All possible $\mathbf{I}_{SR}$ at P are collected. Adding a wavelet (Figure 7b) and possibly other technical parameters to account for various propagation/imaging effects, a so-called *PSDM filter* is generated in the wavenumber domain (Figure 7c). An inverse Fast Fourier Transform (FFT) is applied to this filter to produce the (RB) PSF in the spatial domain (Figure 7d). The PSDM filter can be seen as an equivalent image-processing operator describing the combined effect of propagation and imaging for a scattering structure at P. Its corresponding PSF is an estimation of a point-scatterer response at P as imaged via PSDM.

Figure 8 shows a comparison between the actual point-scatterer response (i.e., PSDM applied to the synthetic data, as in Figure 6) and the response computed from the RB-simulated approach, which assumes a plane-wavefront approximation. As observed, the simulated match with the exact responses at the point scatterer and in its vicinity, but the larger cross-pattern effect is different, being more curved in the exact responses. However, most critical is the response in and around the considered point. RB PSFs are thus already indicative of 3D resolution capabilities of the wave propagation and image construction during the PSDM, allowing quantitative assessment of the vertical and lateral resolution of point scatterers. Moreover, when used in a spatial prestack convolution modeling, RB PSFs are capable of reproducing resolution and illumination effects on PSDM images, i.e., not only for point scatterers but also reflectors (Lecomte et al., 2003). The following examples will illustrate that.

PSDM PSFs are spatially varying, even in a homogeneous background. However, for the sake of simplification, we will assume local targets in the present paper. In other words, we consider the target to be small enough to correspond to a near-constant PSF over the imaged zone. Simulated images will thus be created by convolution between a reflectivity target and one PSF calculated at the center of the image. The analysis of imaging effects will thus be easier. In addition, using a constant PSF over the (local) target allows the spatial convolution to be performed as a multiplication in the wavenumber domain between the PSDM filter and the FFT of the reflectivity. The inverse FFT of that product leads then to the desired spatial image. This is highly efficient and permits near-real-time modeling, which is important for geologists and interpreters who may want to test various models. However, spatial convolution with space-varying (RB) PSFs can also be achieved for larger (full-field) targets but with higher computing cost, although this remains far below the cost of a complete FD modeling followed by imaging. Such full-field convolution can be performed at a later stage, if PSFs calculated over a grid covering the imaging zone indicate clear spatial variability. Prestudies via local-target convolution also help to initiate the modeling parameters for a full-field one.

Figure 9a shows a model with a homogeneous background, and we consider three versions of a (local) target model at the same depth. The first two models consist of isolated point scatterers with different spac-

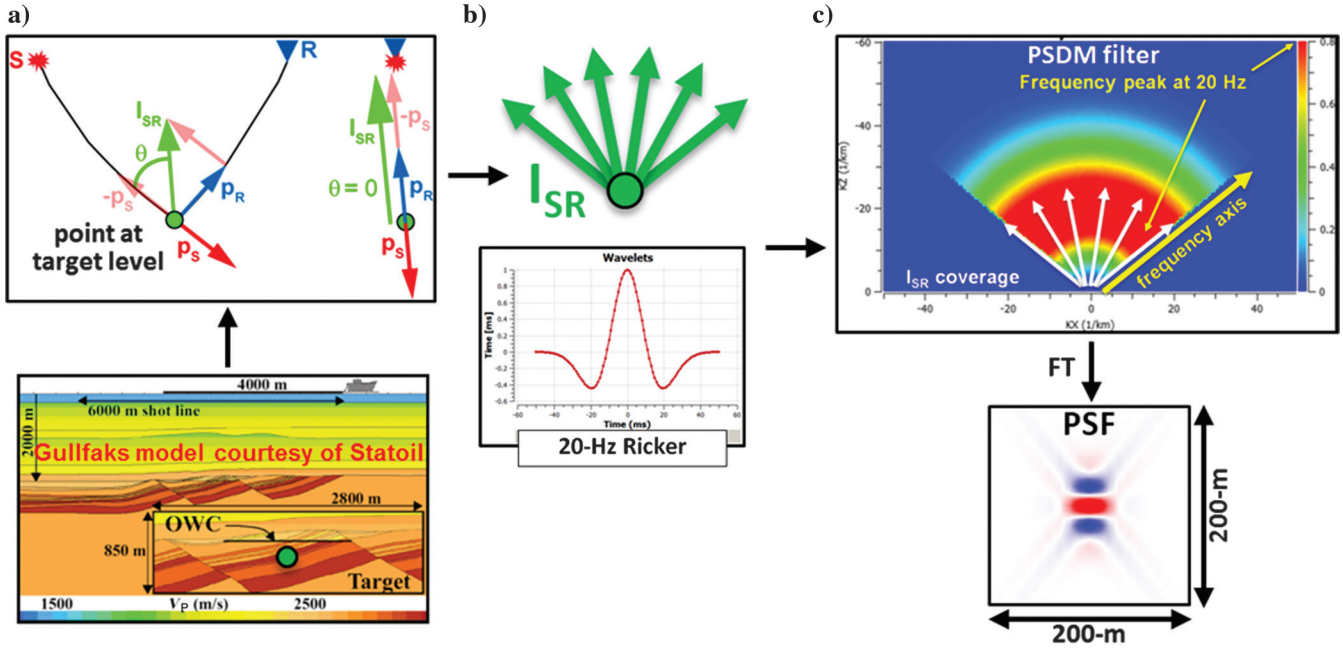

Figure 7. The 3D spatial prestack convolution and basic elements. (a) Velocity model and illumination vector ($\mathbf{I}_{SR}$) defined as the difference between two slowness vectors ($\mathbf{p}_S$ and $\mathbf{p}_R$) for a shot-receiver (SR) couple at a target point (green dot), (b) $\mathbf{I}_{SR}$ for the considered survey and combined with a selected wavelet to generate (c) the equivalent PSDM filter, and (d) the resulting PSF is obtained by Fourier transform of panel (c).

ing between them, and the third is a truncated reflector. Let us consider a survey with a vessel moving from left to right and with two different offsets: 0 and 4 km. This case has no illumination issue; i.e., the truncated reflector will be imaged by both offsets (later examples will illustrate the illumination effects). Figure 9b and 9c shows the corresponding simulated PSDM images. The PSF footprint is visible on the point scatterer models, whereas it is less obvious on the truncated reflector. However, the latter image has to be analyzed as the result of constructive/destructive interference patterns of the PSFs attached to (fictitious) dense point scatterers along the reflector (the second Huygens' principle), the two point-scatterer models being used here to understand such interferences. Following this, and because there is no illumination issue, the migrated energy is focused constructively along the reflector, the PSF footprint explaining the reflector thickness (vertical resolution) and some lateral smearing along it, as seen at the extremities in the far-offset case (lateral resolution). The latter effect explains why faults are not always easily detected as simple discontinuities along reflections. Above and below the reflector itself, the off-center parts of the PSF are expected to interfere destructively, which is observed in Figure 9 due to a regular survey and dense enough S-R distribution. Comparing Figure 9b and 9c also shows the difference in PSFs between zero and far offset. It thus indicates that resolution has to be seen as a survey-dependent 2D/3D pattern. In addition, the zero-offset case shows that resolution is not only a vertical effect, as simplistically modeled by 1D convolution, but also a lateral one.

Let us now illustrate reflector-illumination issues, i.e., which reflectors will be detected by seismic imaging. Figure 10a shows a synthetic case in which a flat horizontal target reflector is below a horizontally layered overburden (above reflector point A) with a salt structure (above reflector point B). In Figure 10b and 10c, PSDM filters and their corresponding PSFs are given for both points. The salt structure strongly influences the illumination of point B, reducing the $\mathbf{I}_{SR}$ coverage at that point, hence a narrow PSDM filter compared with the one at A. As a consequence, a more elongated PSF at B with a different cross pattern is produced (Figure 10b). PSDM filters also directly indicate that the flat reflector at B will not be illuminated, which is explained by its normal (shown by the black vertical arrow in Figure 10b) not being covered by the available $\mathbf{I}_{SR}$ range (arrow outside the orange area), whereas

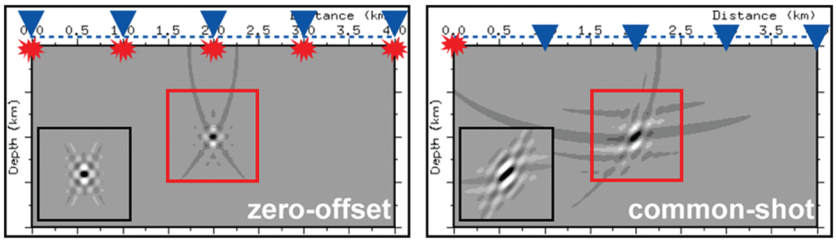

Figure 8. Point-scatterer case of Figure 6. Comparisons between PSDM results (red square) and RB-modeled PSFs (black square), for (left) zero-offset and (right) common-shot configuration.

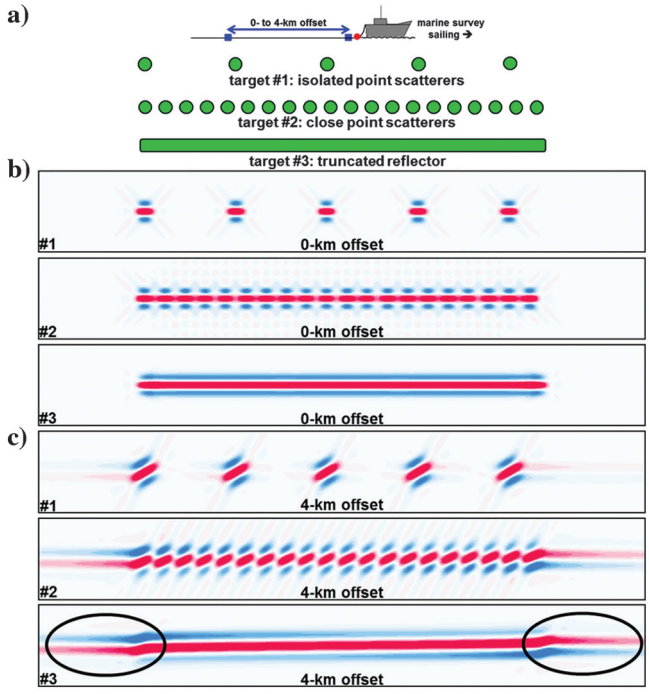

Figure 9. PSF and seismic images. (a) Two point-scatterer models (#1 and #2) and one truncated-reflector model (#3), each model being located at the same depth and illuminated by a marine survey going from left to right; (b) simulated PSDM images for each target model and with a zero-offset acquisition; and (c) same as in panel (b) but with a 4-km offset.

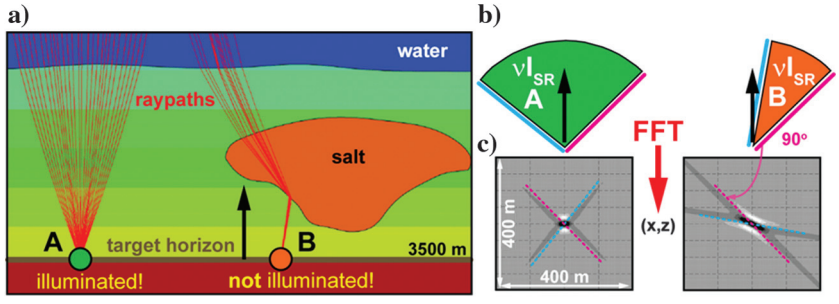

Figure 10. PSF and illumination. (a) Synthetic model: overburden containing a salt body above a flat target reflector (black arrow: normal to the reflector) with two points (A and B) illuminated in a different manner; (b) PSDM filter at A and B, with the normal to the reflector being superimposed (black arrow) in the figure; and (c) corresponding PSFs, the cross-pattern effects (blue and pink lines) being due to the truncation of the filter in panel (b) because of limited illumination vector ($\mathbf{I}_{SR}$) ranges (from Lecomte, 2008a).

in A, there is illumination (arrow inside the green area). This example indicates that seismic illumination is not only a problem for steep dips, as is often assumed. Indeed, at location B, neither the flat reflector nor steeper reflectors dipping left would be detected, whereas steeper reflectors dipping right would be imaged (as long as their normal is within the orange zone). Illumination variability is here due to the survey geometry in combination with wave propagation in the overburden.

Figure 11 illustrates the illumination effect caused only by the survey, by considering one selected reflector from a reservoir model below a homogeneous overburden (Figure 11a). The corresponding reflectivity

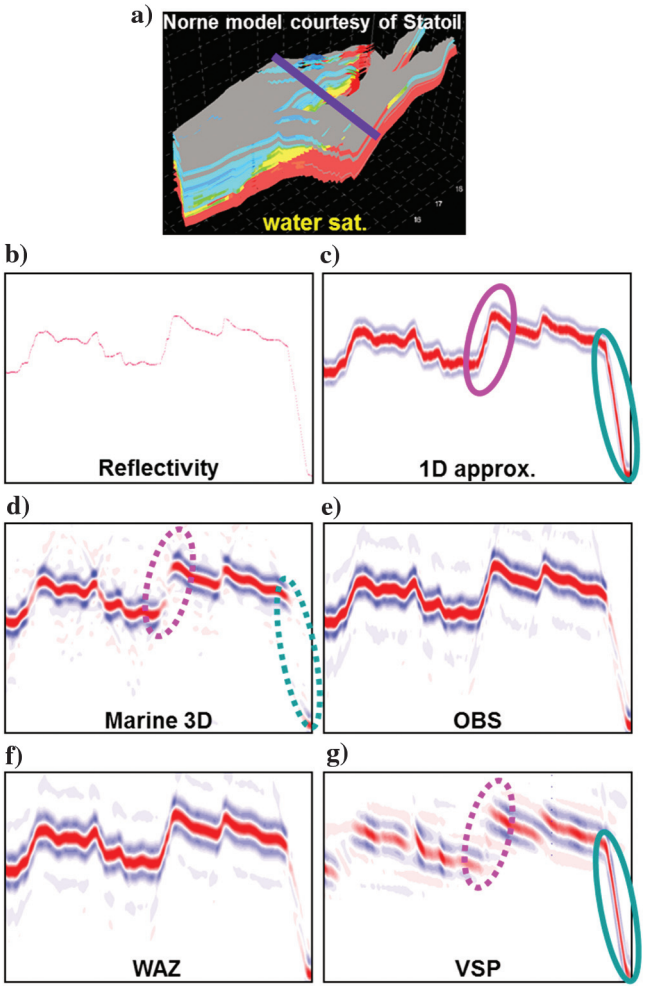

Figure 11. Survey effects. (a) Reservoir model with one of the available parameters prior to seismic modeling and location of a 2D section to image (magenta line); (b) reflectivity section for a selected reflector including faults; (c) 1D trace modeling of the reflector in panel (b); both steep parts (faults, pink and green) are imaged because the modeling cannot deal with illumination issues; (d-g) 3D convolution modeling of the reflector in panel (b) for various surveys: The resolution, off-reflector patterns, and illumination issues vary according to the survey, the steep part (green) being only illuminated by a vertical seismic profile with a well located on the right side of the section.

along that reflector (Figure 11b) is first used as the input of a 1D convolution approach, which does not consider any survey geometry, leading to an "ideal" image of the whole reflector (Figure 11c). In contrast, the simulated images built for standard real survey geometries and computed by 3D convolution of the corresponding PSFs with the same input reflectivity (Figure 11d–11g) show major differences in resolution, off-reflector imaging noise, and illumination. In particular, imaging of the steep reflector parts clearly depends on the survey geometry and its position.

Figure 12 illustrates the importance of accounting for 3D effects in seismic imaging. This figure shows how the same 3D reflectivity cube is seen by seismic imaging if the acquisition consists of a monostreamer 2D line (no crossline resolution at all, which affects the vertical sections by off-side reflections being imaged too), a multistreamer 2D line (some crossline features are roughly perceived, whereas the vertical sections become better resolved), or a 3D multistreamer survey (the crossline structure is now properly imaged). These are, in theory, well-known effects, though they cannot be simulated using only a 1D convolution. Instead, a 3D spatial prestack convolution approach takes into account wave propagation in the overburden in combination with the survey geometry and is much faster than an FD-modeling and processing workflow. The local-target examples shown here took just a few minutes on a standard laptop, a computing time comparable with performing 1D convolution.

So far, the given examples consist of various models, for the target (the zone to image) and for the background/overburden (where the wave propagates). They illustrate the versatility of the RB 3D spatial prestack convolution approach, particularly in comparison with 1D convolution. Before further investigating the effects of seismic-image construction through the use of 3D convolution, we need to discuss the input model itself.

Which geologic models to use?

In standard seismic modeling (either RB or FD), the user starts from a given global velocity model (one model only), defines a seismic survey, chooses a pulse to emit at the source points, and then produces synthetic seismic traces. In such cases, the input velocity model constrains the wave propagation and backscattering of seismic energy. This is also the case for the NIP and IR RB approaches reviewed in the first section for direct poststack modeling. FD methods can deal with arbitrary property grids as models, the cell being the basic property element. RB approaches require instead so-called macromodels, due to the high-frequency assumption, with the elastic properties varying smoothly, possibly between smooth explicit interfaces (at which reflection, transmission, and conversion can be considered), i.e., without geologic details below a few wavelengths (Gjøystdal et al., 2007).

For field-data PSDM, depth imagers first derive a smooth background-velocity model from the seismic re-

cords themselves (e.g., from standard velocity analyses, reflection tomography, etc.). This model is then used to simulate the wave propagation part during the PSDM. After forward modeling, the imaging part of PSDM extracts the backscattered energy contained in the processed data to "map" in depth the reflectors/diffractors onto the initial (smooth) velocity model. In the 3D spatial prestack convolution approach using RB PSFs, we do not calculate synthetic data, which we process/image to get the desired PSDM section. As modelers, we assume that the background velocity model (to calculate the illumination vectors) and a model of the scattering structures (the target to image) are given information. Though these two parts should match where they overlap (in the target), and may indeed be part of the same global model, they are, however, used as two separate entities in the 3D convolution modeling, thus allowing a flexible use of the target model and the background model (e.g., fix one and vary the other).

When dealing with real-data cases, with planned comparisons between actual and modeled seismic, the background velocity model used to generate $\mathbf{I}_{SR}$ should preferably be the smooth one used for PSDM of the actual data. The aim is indeed to reproduce as well as possible the wave-propagation effects contained in the data. In pure synthetic cases, background-velocity models can be of a more general type, especially adapted for RB modeling, e.g., for overburden-related effects with analyses of various wave phases at specific interfaces (e.g., salt bodies). However, the background-velocity model should remain smooth within the target.

The target model used for 3D convolution, on the contrary, can and should be as detailed as possible, being represented on grids as in FD methods. This is a significant advantage compared with standard RB methods and resembles 1D trace modeling, where reflectivity logs can be as detailed as a well log. We should indeed not a priori upscale the properties and let instead the PSF operator automatically perform a "blurring" of the structures according to the wave propagation and frequency content of the wavelet, resolution, and illumination effects combined, as would elastic waves in real cases. Arbitrarily suppressing geologic features in input because supposedly too small according to the "expected" resolution might be damaging.

We can now represent detailed target properties on grids using various inputs. Besides synthetic models used in earlier figures, we have already seen the case of reservoir models (Figures 11 and 12). For computational efficiency of reservoir modeling, these are usually very detailed vertically, but they have lower lateral resolution and are thus not ideal geologic models. Reservoir models are, however, often assigned with sufficient parameters to derive the elastic properties needed to generate the input reflectivity grid, which is a major advantage. Another suitable target input is seismic inversion results because they are already on grids and provide the necessary elastic parameters (e.g., Buland and Omre, 2003).

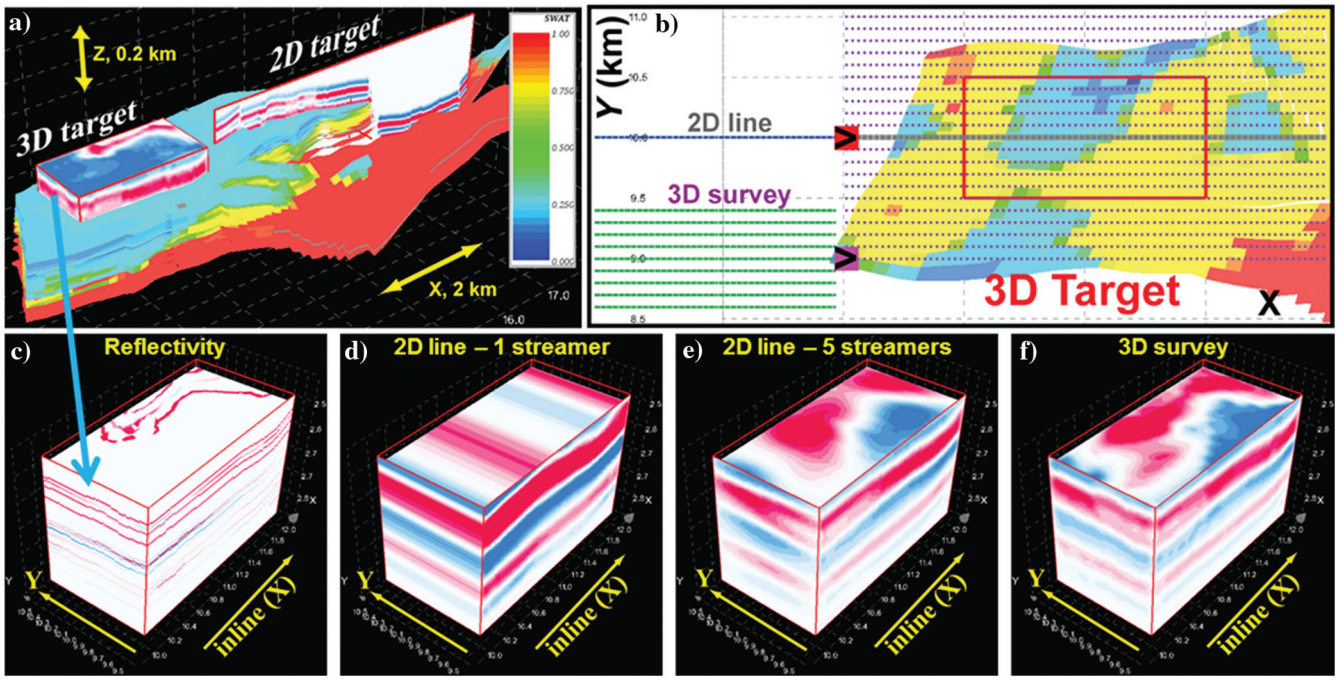

Figure 12. The 3D effects. (a) Reservoir model of Figure 11 with two local targets as examples, the 3D one being used in the following, (b) geometry of 2D/3D surveys, (c) 3D reflectivity structure of the 3D target in panel (a), (d) modeled seismic for the 2D line in panel (b) and one streamer (no crossline resolution), (e) modeled seismic for the same 2D line as panel (d) but with five streamers (coarse crossline resolution), and (f) modeled seismic for the 3D multistreamer survey of panel (b) (proper crossline resolution).

Various geologic models can also be used as target models; e.g., derived from interpretation, outcrop analogs, or any geologic modeling, assuming they can be gridded and populated with proper elastic parameters. Figure 13 is an example of a largely inaccessible cliff section displaying a series of growth faults in the sedimentary succession (Anell et al., 2013; Osmundsen et al., 2014). Digital models, acquired using lidar or photogrammetry analysis of such outcrops (e.g., Buckley et al., 2008), provide detailed spatial geometry of outcrop geologic features and structures, whose interpretation can be used as direct input for modeling. The current analog model of Figure 13 lacks, however, realistic elastic properties. The latter should indeed reflect the expected variations contained in the observed outcrop structures, in combination with some fluids and pressure/temperature conditions of a buried reservoir. Going from outcrop to reservoir models prior to seismic modeling is also a possibility (Rotevatn and Fossen, 2011; Botter et al., 2015), provided that we do not lose too much of the lateral variability due to large pillars, as earlier mentioned. Figure 14 shows 3D numerical modeling of fault zones (Botter et al., 2014a, 2014b), using the 3D spatial convolution to generate seismic cubes from such complex and detailed 3D scattering structures. The elementary spheres of the geomechanical modeling (Figure 14a) are directly mapped on a cube to generate the input reflectivity model (Figure 14b), although one key issue again is assigning proper elastic properties. Finally, Figure 15a and 15b shows actual geologic folds observed at all scales in nature, and Figure 15c shows numerical modeling results of such folds (Schmalholz and Schmid, 2012). Folds provide very interesting geologic structures to model and image (Figure 15d and 15e; see the next section for further analyses of that specific model), even when assuming constant properties within the layers.

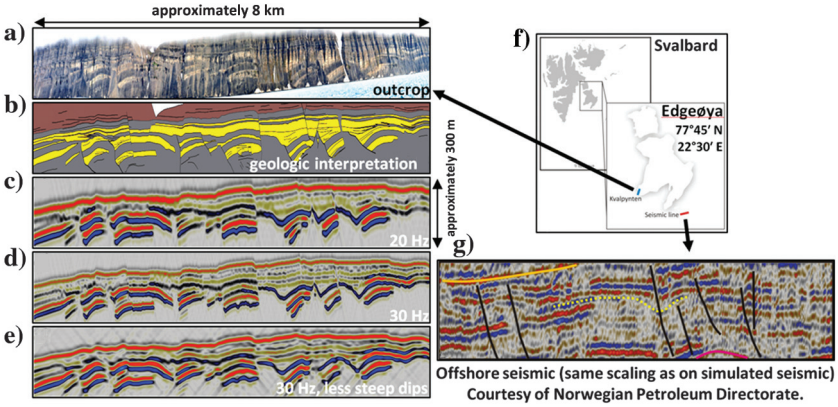

Figure 13. Outcrop modeling. (a) Outcrop analog (Kvalpynten); (b) geologic interpretation; (c-e) modeled PSDM images; (f) location map; (g) Barents sea offshore seismic (similar structures). (c and d) Same illumination pattern, but two different main frequencies; (e) same frequency as in panel (d), but with a more limited illumination pattern (courtesy of TriasNorth project, University of Oslo).

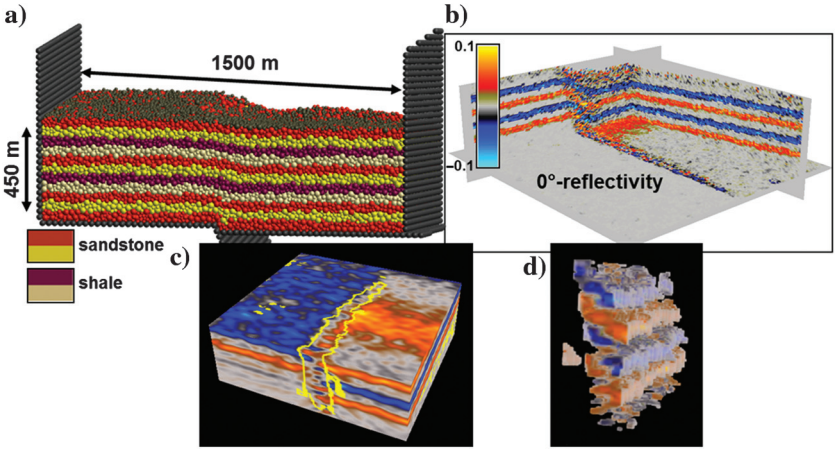

Figure 14. The 3D numerical modeling of fault zones. (a) Geomechanical modeling by the discrete element method for a 3D normal-fault zone with variable displacement along strike, (b) generated reflectivity, (c) 3D convolution modeling of seismic, and (d) automatic attribute extraction (fault zone) from modeled seismic. Figure elements courtesy of C. Botter.

The previous examples show that we now have a large variety of possibilities to define the (local) target model of the 3D spatial prestack convolution approach from detailed geologic structures. This allows seismic modeling of various key near-vertical and/or complex structures known to be problematic in seismic imaging, such as fault zones, gas chimneys, sand injectites, basaltic intrusions, and carbonate reservoirs.

Seismic imaging effects

Seismic modeling of the numerical fold model of Figure 15c was requested by geologists because they suspected that such complex geologic structures, with high dip variations (from flat to vertical), found at all scales and settings in nature, would be represented poorly in seismic images. The geologists wanted to rapidly get synthetic seismic images, not having the resources for exhaustive modeling and processing. The 3D spatial prestack convolution was thus applied, using a complex background-velocity model of a known Norwegian hydrocarbon field and thereby generating the PSF in Figure 15d, which in turn yielded the simulated PSDM image in Figure 15e. This example will be further discussed in later figures, but it already shows how seismic imaging can strongly distort the actual geology, confirming what the geologists suspected, but could not easily demonstrate without modeling.

The latter took just a few minutes on a standard laptop, allowing many parameters to be varied, using the same target model as a reference. In the following, we do not change the target model itself because we want to demonstrate the importance of properly taking into account various parameters influencing a seismic image, i.e., showing that the structure of the target itself is not solely "responsible" for seismic distortions.

1D versus 3D

Figure 16 is used to again demonstrate the shortcomings of 1D trace modeling for actual target structures embedded in any background-velocity model. The velocity model does not even need to be complex for that 1D modeling to fail. Figure 16a is the reflectivity grid used as input for Figure 15e and for all subsequent modeling of the fold model (Figure 15c). An alternating set of positive/negative reflections was assumed by assigning a lower constant velocity in the black layers compared with the white ones. The background velocity model chosen here was homogeneous, for emphasizing target-structure effects and allowing a direct comparison between 1D trace modeling (time domain) and 3D spatial convolution (depth domain), i.e., for avoiding the pulse-stretching effect of PSDM due to velocity variations. One-dimensional trace modeling produces the result displayed in Figure 16b. This result corresponds in a sense to a "1D PSF," i.e., varying only in the vertical direction. Except for the near-vertical parts of the model, we do recognize the folds, with resolution effects being only of a vertical nature. Figure 16c, however, shows a quite different image, where folds are not so easily identified, and with features looking like faults, flat spots, etc. We were using the same frequency content and background velocity of Figure 16b, but now modeling a zero-offset 2D line acquisition above the target, something 1D trace modeling cannot represent. The image changes are then due to the more realistic 2D "footprint" of the combined wave-propagation and image-formation effects (see the corresponding PSF). The smearing of the structures is also lateral and not only vertical, the lateral resolution and cross pattern being partly due to limited-aperture effect. Even in a perfect acquisition case (no limited aperture and all reflector dips illuminated), as in Figure 16d, the resulting PSF would keep a lateral thickness, being a pointlike structure of size defined only by the frequency band and the local velocity. Thus, the corresponding image, though getting closer to folds, still contains imaging artifacts due to the complex interference effects of the (here 2D) PSF along the reflectivity structure.

Frequency and resolution/illumination

A common preconception is that seismic imaging problems can be improved with a high-frequency and/or large-frequency band. This is only partly true because illumination plays an important role too: What is

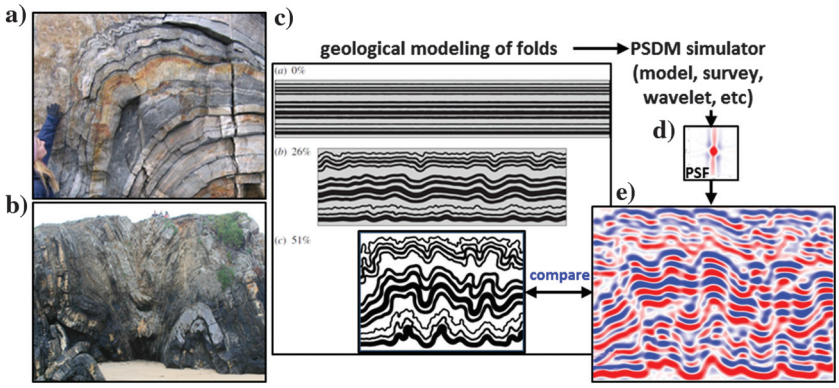

Figure 15. Numeric geologic models. (a and b) Field fold examples, (c) numerical modeling of folds (see Schmalholz and Schmid, 2012), (d) PSF calculated in an actual complex velocity model of the Norwegian Continental Shelf, and (e) simulated PSDM image when applying the PSF in panel (d) to a reflectivity model extracted from panel (c).

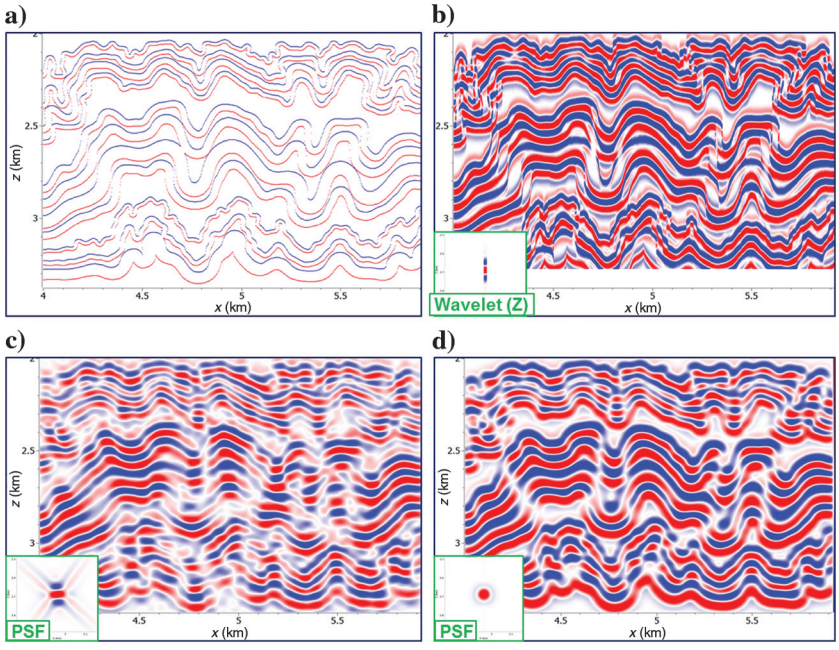

Figure 16. Fold model in homogeneous background. (a) Reflectivity (as used in Figure 15), (b) 1D convolution (depth-converted for comparison), (c) 3D spatial prestack convolution with actual (limited aperture) survey, and (d) 3D spatial prestack convolution with perfect illumination. The same wavelet is used for all modeling experiments, and the PSFs are superimposed in panels (d and c).

not illuminated cannot be seen, whatever the frequency that is used. Figure 17a is equivalent to Figure 16c, whereas Figure 17b uses a much higher dominant frequency. In comparison with the input reflectivity of Figure 16a, the higher frequency yields more structural details, but zones with poor illumination display a very weak signal. With actual data containing various sources of noise, even after processing, the poorly illuminated areas would disappear. Note that the cross pattern of the PSF explains the seismic-image "noise" seen between reflectors and which also exists on actual images. A 1D trace modeling study would miss this interpretation as well as incorporation of illumination effects.

Target location

Figure 18 uses the same homogeneous background velocity model, zero-offset 2D line acquisition, and frequency band as Figure 17a, but the target itself is located at two different depths. For this geometric reason, the $\mathbf{I}_{SR}$ range gets narrower with depth, which induces a decrease in lateral resolution. Although the changes between Figure 18a and 18b may be subtle, there are differences due to the lateral resolution effect. Such "geometric" effects will also occur between sea-surface and sea-bottom acquisitions. One-dimensional trace modeling on the other hand would not reproduce these differences.

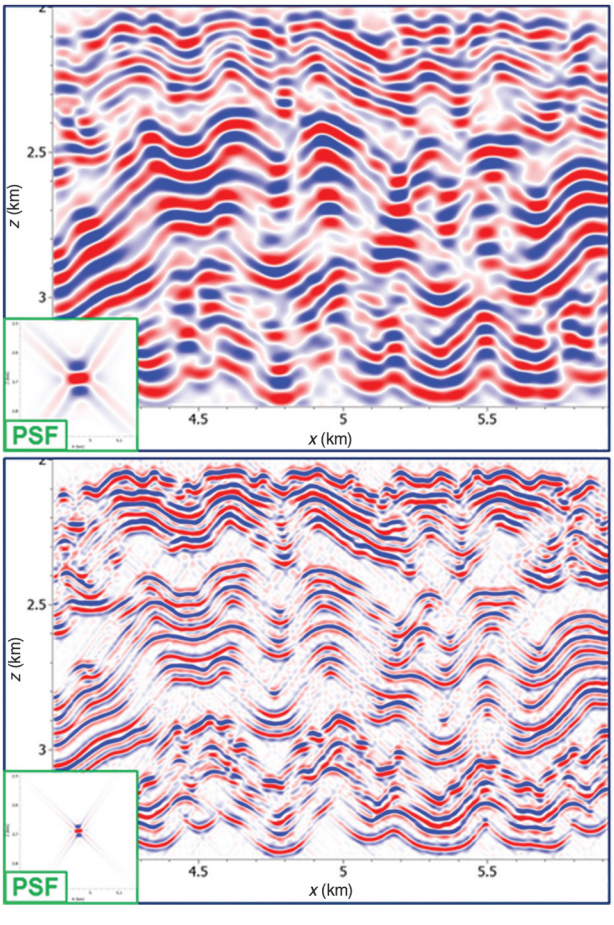

Figure 17. Fold model in homogeneous background and 3D convolution with frequency effects. (a) 10-Hz modeling (same as in Figure 16b) and (b) 30-Hz modeling. The target, depth, and offset are the same for both cases.

Survey and offsets

Figure 19 compares seismic images as seen by a zero offset (Figure 19a) and a larger offset (Figure 19b). The changes on the PSF are a decreasing lateral resolution with increasing offset and also a change in orientation, which indicates a difference in illumination capability. As a result, the seismic images are significantly different. The observed differences in illumination as a function of offset are of great importance when studying amplitude-versus-offset effects.

Background velocity

Finally, Figure 20 compares background-velocity model effects between a homogeneous model and a complex field case (as in Figure 15d), with the zero-offset 2D-line acquisition and the frequency band being the same as in Figures 17a, 18a, and 19a. The differences between these two cases are significant, on PSFs and on the quality of the seismic images, with the overall decrease of resolution in Figure 20b due to the higher velocity in the complex model, and the very different illumination pattern due partly to near-turning waves in the field model. This example helps support the argument that illumination/resolution effects due to the velocity model need to be taken into consideration when interpreting seismic images. This is once more an effect that 1D trace modeling alone cannot take into account.

Discussion

Though a 1D model representation of the earth's structures has been and is still a valuable model for understanding wave propagation, and thus extracting useful information out of seismic data, we should strive to move away from this simplification, even if one is interested in an efficient modeling approach. RB-generated PSFs and their subsequent use in 3D spatial prestack convolution modeling of PSDM sections allow near-interactive assessment of different interpretation models, especially with a local-target version in a first approach (one PSF for the considered imaging zone). The full-field version with space-varying PSFs can then be used to refine the final model. The 3D spatial convolution is also valid in anisotropic cases (Lecomte and Kaschwich, 2008) and accounts for diffraction effects in PSDM (Kaschwich and Lecomte, 2010; Kaschwich et al., 2011). Table 2 summarizes comparison points between 1D and 3D convolution modeling discussed in the present paper and thereby emphasizing the values of 3D versus 1D convolution approaches.

Although computing power continues to improve, the ratio of efficiency between the RB and FD ap-

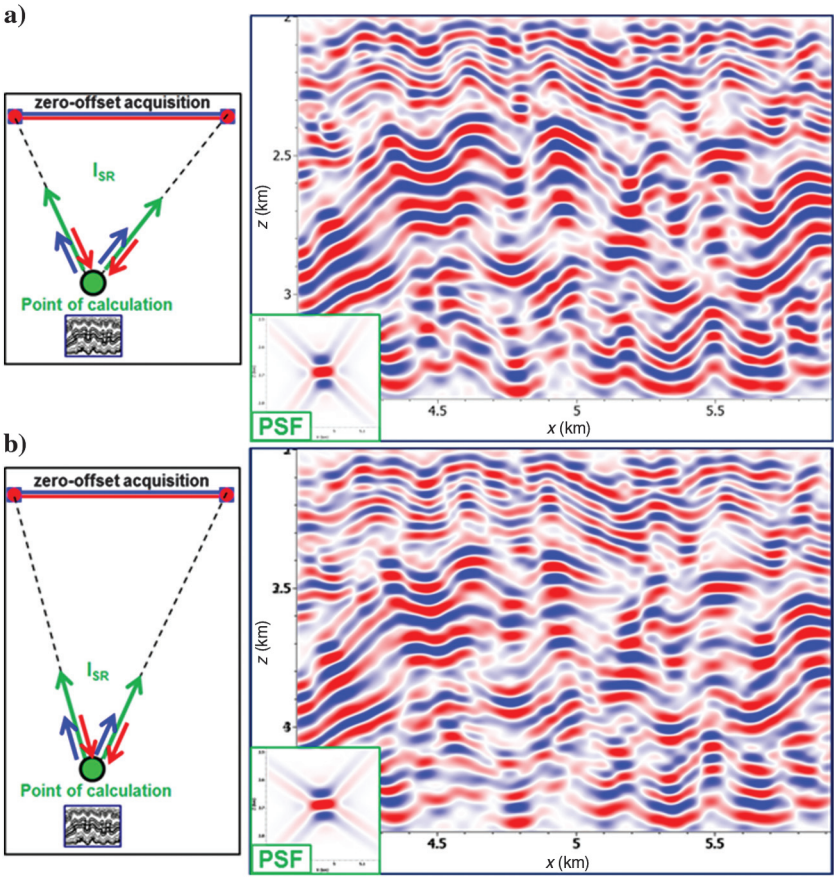

Figure 18. Fold model in a homogeneous background: 3D convolution with depth effects. (a) Shallow depth and (b) deeper depth. The same target, offset, and wavelet are used for both cases.

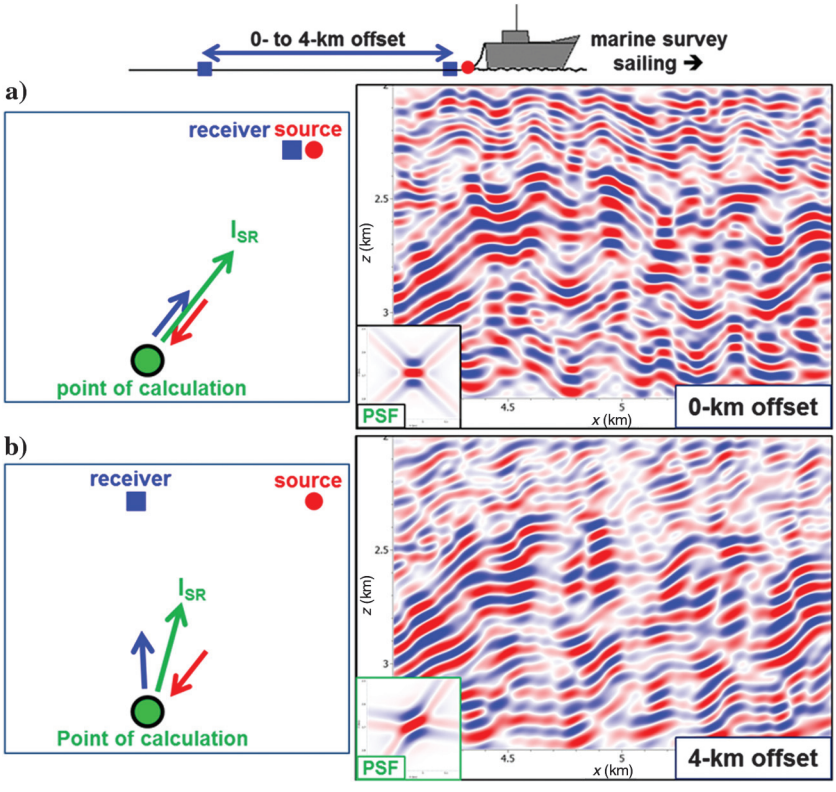

Figure 19. Fold model in homogeneous background: 3D convolution with offset effects. (a) Small offset and (b) large offset. The same target, depth, and wavelet are used for both cases.

proaches will remain, RB modeling being a more efficient and less demanding method. However, benchmarking with FD-modeled cases of various complex structures requiring PSDM imaging is a necessity and could help to further improve RB-generated PSFs.

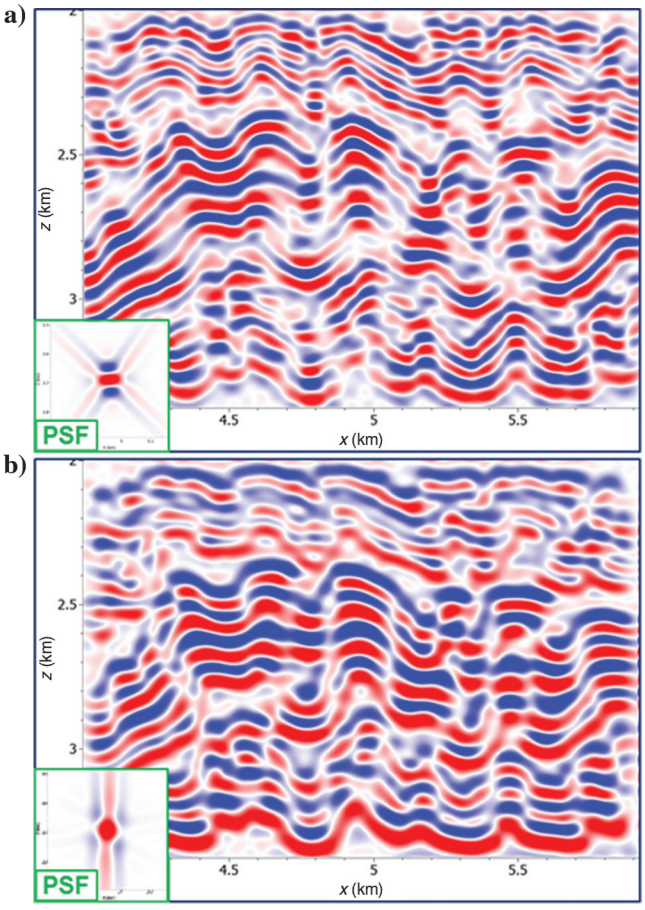

Figure 20. Fold model in different background velocity fields. (a) Homogeneous background and (b) actual velocity field of the Norwegian Continental Shelf. The same target, depth, offset, and wavelet are used for both cases.

One key assumption made for the latter is a locally plane-wavefront approximation, which explains the increasing mismatch of the cross patterns in Figure 8 further away from the center (curved in actual PSDM and straight in RB-modeled PSFs). However, RB methods also give the necessary parameters for such curvature effects (Gelius et al., 2002), and adding them would be straightforward without a significant increase in computation time. Implementing this would also give a better match of the migration noise generated by the cross patterns of the PSF (limited-aperture effect) and due to imperfect interferences of the scattering isochrones during imaging. Finally, though the RB-generated PSFs are especially designed to simulate Kirchhoff-type migration results, we believe in adding specific preprocessing of the PSDM filters to generate PSFs more closely suiting full-wavefield migration images.

Key inputs in all modeling discussed earlier are proper elastic parameters to obtain realistic reflectivity. Although this major issue has not been specifically addressed here, it does remain a troublesome point if one wishes to provide geologists and interpreters with easy-to-use and efficient modeling tools, without getting involved in complicated (e.g., rock physics) modeling. It is indeed important to use adequate values of velocities and density, and defining proper S-wave velocities too, even if dealing with P-wave seismic (e.g., Øygarden et al., 2015).

Industry-standard seismic inversion is still guided by 1D convolution modeling. Moving toward inversion using a 3D convolution operator for the modeling part is, however, now possible with RB (or FD) PSFs. First-use attempts of RB PSFs for better wavelet estimation have been published elsewhere (Georgsen et al., 2010). In addition, turning the 1D inversion itself into a 3D RB-PSF constrained inversion, following the Buland and Omre (2003) inversion scheme, is also prototyped but not yet published because thorough testing toward benchmarked synthetics and actual PSDM data remain to be completed. Similarly, using a full-wavefield approach, Letki et al. (2015) recently show that FD PSFs

Table 2. Comparison between 1D and 3D convolution modeling.

	1D time poststack convolution	3D spatial poststack convolution
Features and applications	Reflectivity and wavelet as input	Reflectivity and wavelet as input
	No propagation effects taken into account	Propagation effects, with velocity model, survey, and other parameters
	Strictly limited to 1D models, i.e., vertical variations only	No model limitations, accepting lateral velocity variations
	Fastest and robust	Fast and robust
	Simulates poststack time-migrated images	Simulates PSDM images
	Vertical time (1D) resolution	3D spatial resolution
	No illumination effects	3D illumination effects
	Limited sensitivity analyses	Various sensitivity analyses

can compensate for illumination effects in a depth-domain inversion approach, giving better amplitudes leading to improved interpretation.

Conclusions

Although 1D convolution modeling has been key to seismic acquisition, processing, imaging, and inversion developments, it is time to reconsider its use, especially when dealing with complex earth structures requiring PSDM and more advanced interpretations. However, in such cases, it is not necessary to move directly from 1D convolution to FD modeling, the latter nevertheless being a requirement for producing complete synthetic data for advanced processing developments in complex models. A middle ground of RB modeling has proven to fill gaps in modeling needs by developing a 3D spatial prestack convolution approach. It allows more realistic modeling than 1D convolution for geologists and interpreters, assuming that the users take into account additional input elements, such as velocity models, survey geometry, and other acquisition/processing parameters. Being able to provide good estimates of PSDM PSFs, in a flexible manner, and using them for 3D convolution with detailed target structures, makes RB modeling an improved method to increase understanding and allow analysis of various effects affecting seismic images. Although FD modeling can also produce PSFs for such 3D convolutions, RB modeling remains faster, more flexible and interactive; hence, it is more accessible for routine work. However, work remains to further improve RB-modeled PSFs, especially toward amplitude calibration and simplify modeling workflows for use in seismic interpretation.

Acknowledgments

The Research Council of Norway (RCN) is acknowledged for yearly basic funding supporting research activities within seismic modeling and imaging at NORSAR, and for project grant #234152 lead by the University of Oslo (Figure 13; "TriasNorth" project cosponsored by DEA, Edison, Lundin, Statoil, and Tullow). We are very grateful to three anonymous reviewers and associate editor Carlos Calderón for their thorough reviews and useful corrections/comments. The two first authors thank all NORSAR research and development colleagues and programmers in the seismic modeling department. Thanks also go to C. Botter for Figure 14, as part of her Ph.D. work on "Seismic imaging of fault zones" (RCN-Petromaks project, grant no. 210425/E30). Seismic Unix was used for some of the cases and figures, especially to generate reference data sets.

References

Anell, I., A. Braathen, S. Olaussen, and P.T. Osmundsen, 2013, Evidence of faulting contradicts a quiescent northern Barents Shelf during the Triassic: First Break, **31**, 67–76.

Anselmetti, F. S., G. P. Eberli, and D. Bernoulli, 1997, Seismic modeling of a carbonate platform margin (Montagna della Maiella, Italy): Variations in seismic facies and implications for sequence stratigraphy, *in* F. J. Marfurt, and A. Palaz, eds, Carbonate seismology, Geophysical Development Series: SEG, 373–406.

Arntsen, B., L. Wensaas, H. Løseth, and C. Hermanrud, 2007, Seismic modeling of gas chimneys: Geophysics, **72**, no. 5, SM251–SM259.

Behzad, A., 2012, Seismic modeling of complex geological structures, *in* M. Kanao, ed., Seismic waves — Research and analysis: InTech, 213–236.

Black, J. L., and M. A. Brzostowski, 1994, Systematic of time-migration errors: Geophysics, **59**, 1419–1434, doi: 10.1190/1.1443699.

Botter, C., N. Cardozo, S. Hardy, I. Lecomte, and A. Escalona, 2014a, From mechanical modeling to seismic imaging of faults: A synthetic workflow to study the impact of faults on seismic: Marine and Petroleum Geology, **57**, 187–207, doi: 10.1016/j.marpetgeo.2014.05.013.

Botter, C., N. Cardozo, S. Hardy, I. Lecomte, A. Escalona, N. Cooke, and G. Paton, 2014b, From geomechanical modelling to seismic imaging of 3D faults: 76th Annual International Conference and Exhibition, EAGE, Extended Abstracts, A104 09.

Botter, C., N. Cardozo, I. Lecomte, A. Rotevatn, and G. Paton, 2015, The effect of fluid flow in relay ramps on seismic images: 4th International Conference on Fault and Top Seals, EAGE, Extended Abstracts, Mo FTS 05.

Buckley, S. J., J. A. Howell, H. D. Enge, and T. H. Kurz, 2008, Terrestrial laser scanning in geology: Data acquisition, processing and accuracy considerations: Journal of the Geological Society, **165**, 625–638, doi: 10.1144/0016-76492007-100.

Buland, A., and H. Omre, 2003, Bayesian linearized AVO inversion: Geophysics, **68**, 185–198, doi: 10.1190/1.1543206.

Fagin, S. W., 1991, Seismic modeling of geologic structures: Applications to exploration problems, Geophysical Development Series: SEG.

Gelius, L.-J., I. Lecomte, and S.-E. Hamran, 2002, The concept of local parabolic wave imaging (LpI) in PSDM: 72nd Annual International Meeting, SEG, Expanded Abstracts, 1184–1187.

Georgsen, F., O. Kolbjørnsen, and I. Lecomte, 2010, A 3D ray-based pulse estimation for seismic inversion of PSDM data: 72nd Annual International Conference and Exhibition, EAGE, Extended Abstracts, A031.

Gjøystdal, H., E. Iversen, I. Lecomte, T. Kaschwish, Å. Drottning, and J. Mispel, 2007, Improved applicability of ray tracing in seismic acquisition, imaging, and interpretation: Geophysics, **72**, no. 5, SM261–SM271, doi: 10.1190/1.2736515.

Gray, S. H., 2001, Seismic imaging: Geophysics, **66**, 15–17, doi: 10.1190/1.1444892.

Hubral, P., 1977, Time-migration: Some ray-theoretical aspects: Geophysical Prospecting, **25**, 738–745, doi: 10.1111/j.1365-2478.1977.tb01200.x.

Johansen, S., E. Granberg, D. Mellere, B. Arntsen, and T. Olsen, 2007, Decoupling of seismic reflectors and stratigraphic timelines: A modeling study of Tertiary strata from Svalbard: Geophysics, **72**, no. 5, SM273–SM280, doi: 10.1190/1.2759479.

Kaschwich, T., H. Gjøystdal, and I. Lecomte, 2011, Impact of diffraction on resolution of PSDM: 73rd Annual International Conference and Exhibition, EAGE, Extended Abstracts, P384.

Kaschwich, T., and I. Lecomte, 2010, Improved ray-based seismograms by combining modeling by demigration with a prestack depth migration simulator: 72nd Annual International Conference and Exhibition, EAGE, Extended Abstracts, C041.

Laurain, R., L.-J. Gelius, V. Vinje, and I. Lecomte, 2004, A review of 3D illumination studies: Journal of Seismic Exploration, **13**, 17–37.

Lecomte, I., 2006, Fremgangsmåte for simulering av lokale prestakk dypmigrerte seismiske bilder: Norway Patent 322089.

Lecomte, I., 2008a, Resolution and illumination analyses in PSDM: A ray-based approach: The Leading Edge, **27**, 650–663, doi: 10.1190/1.2919584.

Lecomte, I., 2008b, Method simulating local prestack depth migrated seismic images: U.S. Patent 7,376,539.

Lecomte, I., 2013a, Method for simulating local prestack depth migrated seismic images: Canada Patent 2,521,919.

Lecomte, I., 2013b, Method for simulating local prestack depth migrated seismic images: European Patent 1611461, validated in France, Germany, The Netherlands, and United Kingdom.

Lecomte, I., and L.-J. Gelius, 1998, Have a look at the resolution of prestack depth migration for any model, survey and wavefields: 68th Annual International Meeting, SEG, Expanded Abstracts, 1112–1115.

Lecomte, I., H. Gjøystdal, and Å. Drottning, 2003, Simulated prestack local imaging: A robust and efficient interpretation tool to control illumination, resolution, and time-lapse properties of reservoirs: 73rd Annual International Meeting, SEG, Expanded Abstracts, 1525–1528.

Lecomte, I., and T. Kaschwich, 2008, Closer to real earth in reservoir characterization: A 3D isotropic/anisotropic PSDM simulator: 78th Annual International Meeting, SEG, Expanded Abstracts, 1570–1574.

Letki, L. P., J. Tang, and X. Du, 2015, Depth domain inversion case study in complex subsalt area: 77th Annual International Conference and Exhibition, EAGE, Extended Abstracts, N104 12.

Osmundsen, P. T., A. Braathen, R. S. Rød, and I. B. Hynne, 2014, Styles of normal faulting and fault-controlled sedimentation in the Triassic deposits of Eastern Svalbard: Norwegian Petroleum Directorate Bulletin, **11**, 61–79.

Øygarden, B., H. Løseth, and S. Njerve, 2015, Rock properties of smectite- and ooze-rich claystones: Geophysics, **80**, D89–D98, doi: 10.1190/geo2013-0363.1.

Pangman, P., 2007, SEAM launched in March: The Leading Edge, **26**, 718–720, doi: 10.1190/tle26060718.1.

Podvin, P., and I. Lecomte, 1991, Finite difference computation of traveltimes in very contrasted velocity models: A massively parallel approach and its associated tools: Geophysical Journal International, **105**, 271–284, doi: 10.1111/j.1365-246X.1991.tb03461.x.

Robinson, E. A., and S. Treitel, 1978, The fine structure of the normal incidence synthetic seismogram: Geophysical Journal of the Royal Astronomical Society, **53**, 289–309, doi: 10.1111/j.1365-246X.1978.tb03743.x.

Rotevatn, A., and H. Fossen, 2011, Simulating the effect of subseismic fault tails and process zones in a siliciclastic reservoir analogue: Implications for aquifer support and trap definition: Marine and Petroleum Geology, **28**, 1648–1662, doi: 10.1016/j.marpetgeo.2011.07.005.

Schmalholz, S. M., and D. W. Schmid, 2012, Folding in power-law viscous multi-layers: Philosophical Transactions of the Royal Society A: Mathematical, Physical, and Engineering Sciences, **370**, 1798–1826, doi: 10.1098/rsta.2011.0421.

Schneider, W. A., 1978, Integral formulation for migration in two and three dimensions: Geophysics, **43**, 49–76, doi: 10.1190/1.1440828.

Sen, M., 2014, Seismic, reflectivity method, *in* H. Gupta, ed., Encyclopedia of solid earth geophysics: Springer, 1269–1279.

Toxopeus, G., S. Petersen, and K. Wapenaar, 2003, Improving geological modeling and interpretation by simulated migrated seismics: 65th Annual International Conference and Exhibition, EAGE, Extended Abstracts, F34.

Isabelle Lecomte received M.S. (1987), Civ. Eng. (1988), and Ph.D. (1990; IFREMER grant) degrees, all in geophysics from the University of Strasbourg, France. In 1991–1992, she was a postdoctoral fellow at NORSAR, Norway (grants from EU, 1991; Research Council of Norway, 1992). She joined NORSAR permanently in 2003 as senior research geophysicist in R&D seismic modeling, and she is now principal research geophysicist. In 2003–2012, she was a part-time researcher at the International Centre for Geohazards (Oslo), coordinating geophysics. Since 2012, she has been an adjunct associate professor at Oslo University, Norway, teaching near-surface geophysics. She received the 2001 EAGE Loránd Eötvös award and the 2014 Norwegian Geophysical award. Her main research interests include seismic modeling and imaging, with applications to seismic reflection, refraction, tomography, resolution, and simulation of PSDM.

Paul Lubrano Lavadera received M.S. (2009), Civ. Eng. (2009), and Ph.D. (2013) degrees, all in geophysics from the University of Strasbourg, France. He is a postdoctoral research fellow at NORSAR, Norway (2014–present). His research interests include geothermal, microseismics, seismic modeling, and imaging.

Ingrid Anell received a Ph.D. (2010) in geology from the University of Copenhagen, Denmark. She is a postdoctoral candidate with the Triassic North project at the University of Oslo. Her research interests include interpretation of seismic data, offshore geometries of sedimentary features, and links to onshore depositional environments.

Simon Buckley received B.S. (1999) and Ph.D. (2003) degrees in geomatics from Newcastle University, UK, and has had postdoctoral positions at the University of Newcastle, Australia, and the University of Bergen, Norway. He is a senior researcher at Uni Research CIPR, Bergen, Norway. His research interests include developments of geomatics methods, such as laser scanning and photogrammetry, in geoscience applications.

Daniel W. Schmid received a Ph.D. (2002) in geology from the ETH Zurich, Switzerland. He is working as a researcher at the Department of Geosciences, University of Oslo, and as a consultant and software developer for the oil industry. His main areas of expertise are structural geology, geomechanics, and petroleum system modeling.

Michael Heeremans received a Ph.D. (1997) in structural geology and tectonics from the Vrije Universiteit, Amsterdam, Netherlands. He started as a postdoctoral fellow (1997–2001) at the University of Oslo, Norway, followed by a research position (2002–2008). Since 2008, he has been working there as a senior engineer, and his main focus has been on research-related IT support. He has been teaching seismic interpretation for more than 10 years.